ELSEVIER

Surface Science 335 (1995) 110–119

surface science

Classification of growth behaviour for copper on various substrates with in-situ scanning probe microscopy

Richard J. Nichols [a], Elke Bunge [b,*], Heinrich Meyer [b], Helmut Baumgärtel [c]

[a] *Department of Chemistry, The University of Liverpool, Liverpool L69 3BX, UK*
[b] *Atotech Deutschland GmbH, Erasmusstrasse 20-24, 10553 Berlin, Germany*
[c] *Freie Universität Berlin, Takustrasse 3, 14195 Berlin, Germany*

Received 11 October 1994; accepted for publication 24 April 1995

Abstract

In-situ scanning probe microscopy has been used to directly examine the deposition of copper on gold, polypyrrole and gold substrates which have been precovered with a multilayer copper film. The growth of the copper deposits, from electrolytes with and without additives, have been classified for these different substrates in accordance with Bauer [1] as either: (A) the Stranski–Krastanov mechanism involving the deposition of one or more layers followed by the formation of three-dimensional islands; (B) Frank–van der Merwe layer-by-layer growth of either individual monolayers (B_1); or *multilayer films* (B_2); or (C) the Volmer–Weber mechanism involving the formation of bulk islands directly on-top of the substrate.

We show that the growth behaviour can be rationalised in terms of simple thermodynamic models which take into account, the strength of the deposit–substrate interaction and the crystallographic misfit between the deposit and the underlying substrate surface.

Keywords: Atomic force microscopy; Copper; Gold; Growth; Nucleation; Scanning tunneling microscopy; Single crystal surfaces; Solid–liquid interfaces

1. Introduction

The electrocrystallisation of metallic deposits on foreign substrates continues to be studied intensively. This is a reflection of its fundamental importance in technology and industry as well as in science. The dependence of the nucleation and growth of the deposit on the deposition conditions is of particular interest. However, these processes are quite complex since many parameters can play a role including deposit–substrate interactions, substrate structure and crystallographic orientation, current density and electrode potential, adsorbates, electrolyte composition, mass transport and temperature. Inspite of this complexity much progress has been made in recent years, particularly owing to the application of conventional electrochemical and modern surface analytical techniques to model systems.

One of the newer techniques for examining electrode surfaces is scanning probe microscopy (SPM). The scanning probe microscopies, in particular scanning tunnelling microscopy (STM) and atomic force microscopy (AFM), have had a major impact in the investigation of metal ad-layer formation and in the

* Corresponding author.

SSDI 0039-6028(95)00578-1

investigation of the nucleation and growth behaviour of metal deposits at overpotentials [2].

The primary goal of this paper is to classify the growth of bulk copper deposits on various substrates and to rationalise the observed growth modes. Possible thermodynamic origins we have considered are deposit–substrate interaction and the strain energy of the deposit. The classification scheme used here was developed some time ago by Bauer [1]. The scheme presented by Bauer distinguishes between three basic growth modes (Fig. 1): the Stranski–Krastanov mode (A); the Frank–van der Merwe mode (B) and the Volmer–Weber mode (C). In addition we have divided the Frank–van der Merwe growth mode into two; namely monolayer film growth (B_1) and multilayer film growth (B_2), as has been discussed by Budevski [3]. In accordance with the description of Bauer, the Volmer–Weber mode (C) should be typically observed whenever the deposit–substrate interaction is weak compared to the deposit–deposit interaction, in other words whenever the surface energy of the deposit material is large compared to that of the substrate. The other two modes (A and B) should be observed for the reverse case; i.e. a relatively strong deposit–substrate interaction. The film would be expected to grow by the Frank–van der Merwe mechanism (B) if the strain energy of the deposited film is small or non-existent (homo-epitaxy). On the other hand, if an appreciable strain exists then the Stranski–Krastanov mode should occur.

The aforementioned growth modes have been developed and most comprehensively examined for deposition from the gas phase [4]. The situation is somewhat more complicated for the electrodeposition of metals where other parameters also play a role. However, it has been previously recognised that the metal ad-atom–substrate interaction and crystal-

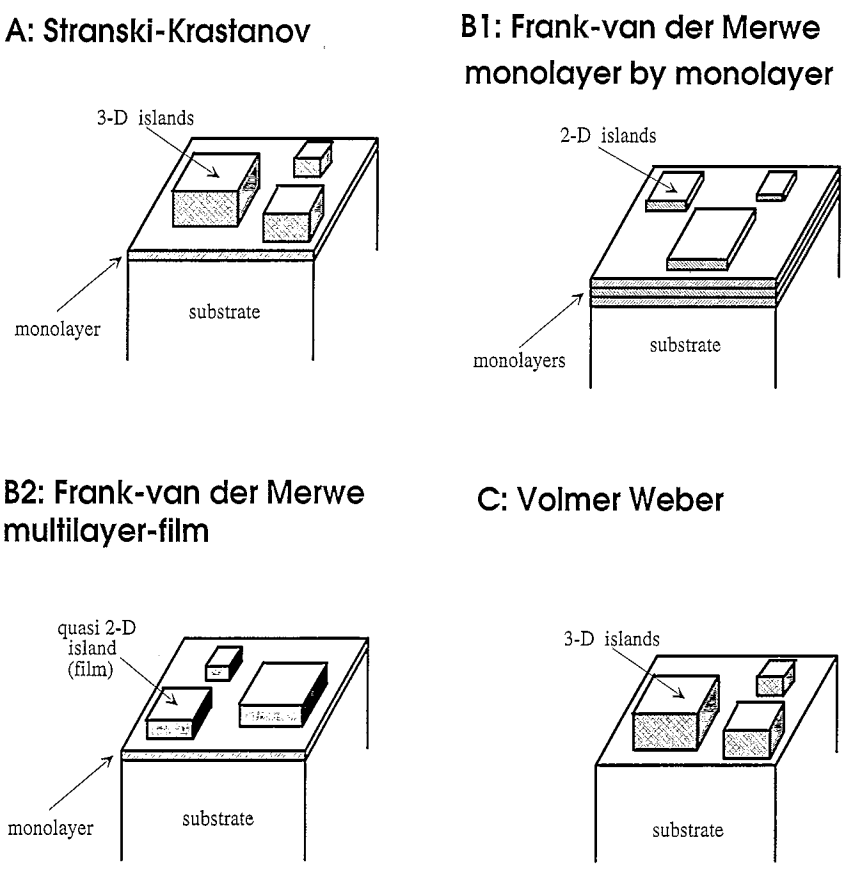

Fig. 1. Classification used here for the different types of growth.

lographic misfit are also of particular importance in the electrodeposition process [5,6]. In systems where underpotential deposition (UPD) phenomena occur, such as $Cu^{2+}/Au(hkl)$, the transition between the underpotential deposit and the overpotential deposit (OPD) is of particular interest. In such cases the underpotentially deposited metal adlayer acts as a precursor for the nucleation and growth of the overpotential deposit [5,6]. The structures of underpotentially deposited copper ad-layers on Au(*hkl*) have been studied intensively in recent years using a variety of methods including scanning probe microscopies [2,7–10].

2. Experimental

A well-defined Au(111) single crystal was used for the conventional electrochemical measurements, while gold on glass samples were used for the SPM measurements. Both samples were prepared by the well-known flame annealing method to yield (111) surfaces [11,14].

The cyclic voltammetry measurements were performed with a EG & G (PAR273) potentiostat and capacitance measurements with an impedance unit from Zahner Electric (IM5d). In the latter case the potential was stepped in 25 mV divisions with an AC perturbation of 5 mV amplitude at 80 Hz. The in-situ STM imaging was performed with a Nanoscope II STM with a bipotentiostat and the in-situ AFM measurements with a Nanoscope III. Details of the in-situ STM and AFM experiments have been described elsewhere [12,13]. The particular experimental considerations for studying bulk metal deposition processes in-situ with STM or AFM have also been previously discussed [2,12]. All potentials quoted for the conventional electrochemical

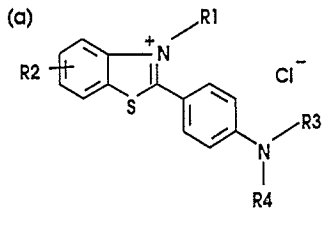

Fig. 2. The additive investigated here.

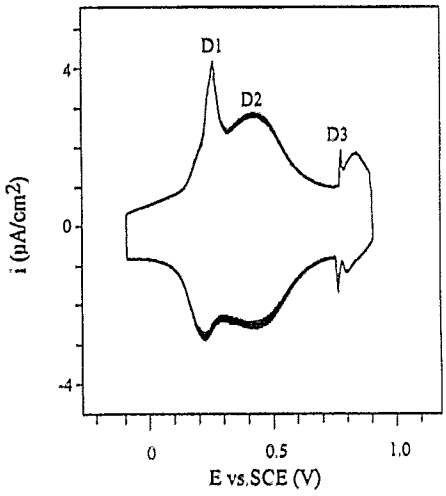

Fig. 3. A cyclic voltammogram of Au(111) in 0.1M H_2SO_4. Potentials vs. SCE, scan rate 0.02 V/s.

measurements are versus a saturated calomel reference electrode (SCE). In the case of the in-situ STM and AFM measurements it was more convenient to use a copper wire as the reference electrode and hence these measurements are quoted with respect to the Cu/Cu^{2+} reference electrode.

For the purpose of examining the initial stages of copper deposition on polypyrrole we have chosen an intrinsically conductive polypyrrole film (polypyrrole benzenesulfonate from BASF, Lutamer® ES 9567). The film (ca. 35 μm thick, conductivity 150 S cm^{-1}) is electrochemically synthesised and contains no fillers.

Benzothiazonium derivative, the additive discussed here, is shown in Fig. 2. This additive was purified by recrystallization. The electrolytes were prepared from doubly distilled water, $CuSO_4$ (Merck, p.a.) and H_2SO_4 (Merck, suprapur).

3. Results and discussion

3.1. Electrochemical measurements

Electrochemical measurements were used to characterise the adsorption of the organic additive BT-B and the underpotential deposition of Cu on Au(111) in the presence of the additive.

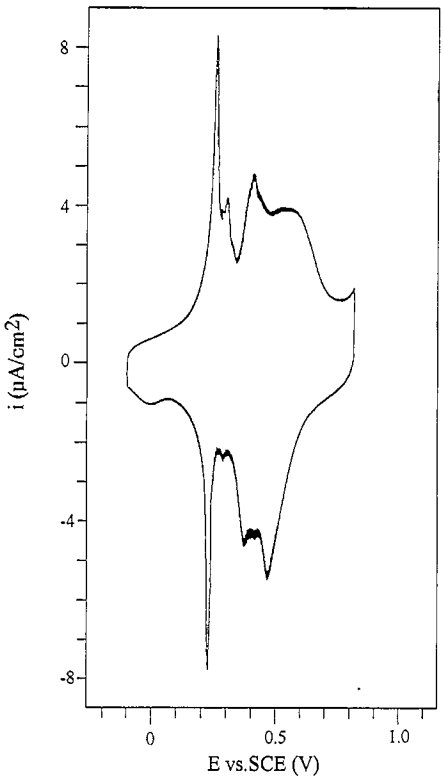

Fig. 4. A cyclic voltammogram of Au(111) in 0.1M H_2SO_4 with 3×10^{-4}M BT-B. Potentials vs. SCE, scan rate 0.02 V/s.

3.1.1. Cyclic voltammetry and capacitance measurements of Au(111) in sulphuric acid electrolytes with and without BT-B

A cyclic voltammogram of Au(111) in 0.1 H_2SO_4 in the potential window from −0.1 to 0.9 V is shown in Fig. 3. This voltammogram is in good agreement with that previously reported in the literature [15]. Three distinctive peaks have been marked in accordance with the notation of Ref. [15]. The peaks have been assigned to various steps of the adsorption/desorption of sulphate and/or bisulphate anions. This potential region is also marked by a reversible reconstruction of the surface from $(22\times\sqrt{3})\leftrightarrow(1\times1)$. These phenomena have been discussed in detail in other papers [16–20].

A similar voltammogram is seen in Fig. 4, but this time with the addition of 3×10^{-4}M BT-B. In this case four distinctive peaks are observed: a sharp peak at 0.230 V and the other peaks at 0.285, 0.380 and 0.515 V, respectively. The latter two peaks are rather similar in terms of shape and form to peaks D_1 and D_2, although they are shifted by about 120 and 95 mV in the positive direction. The similar shape and form of these peaks to D_1 and D_2 suggests an analogous mechanism for the lifting of the reconstruction. An explanation for the shift of these peaks to more positive potentials, is that the reconstructed surface is stabilised by the adsorbate and a more positive potential must be reached before the reconstruction is lifted. The peak separation between these latter peaks is nevertheless somewhat smaller (135 mV) compared to the peaks D_1 and D_2 in the pure solution (160 mV). However, the most significant differences between the voltammetry upon addition of BT-B are the appearance of the very sharp predominant peak at 0.230 V and the absence of a peak similar to D_3. The sharp peak has a full width at half height of less than 15 mV and may be indicative of a phase transition of the adsorbed organic film (and/or coadsorbed Cl^-), although this hypothesise cannot be verified at the moment. It is also not clear whether peak D_3 is totally suppressed or whether it is shifted to more positive potentials, where it would be difficult to distinguish from the beginning of surface oxidation. The potential scans were not extended to more positive potentials to avoid the risk of undesirable restructuring of the surface due to surface oxidation and also to avoid oxidation of the organic adsorbate.

The adsorption of the additive BT-B on Au(111) was investigated in greater detail by capacitance measurements. Fig. 5 shows capacitance versus potential measurements of 0.1M H_2SO_4 without and

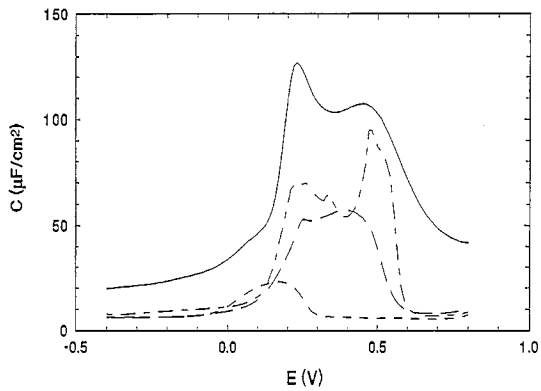

Fig. 5. Capacitance versus potential measurements of Au(111) in 0.1M H_2SO_4 and xM BT-B. (a) $x=0$ (———); (b) $x=1\times10^{-5}$ (— - —); (c) $x=3\times10^{-4}$ (— —); (d) $x=1\times10^{-3}$ (– – –).

with the addition of various aliquots of BT-B. The addition of BT-B leads to a very substantial decrease in the capacitance with respect to the curve obtained in the sulphuric acid base electrolyte. Within the range of BT-B concentrations investigated, the capacitance decreases as the concentration of additive is increased. The capacitance is markedly decreased over the complete potential region from −0.4 to 0.8 V. This indicates that the additive is adsorbed to a certain extent over this whole potential range. In the potential range between −0.4 and 0.05 V the capacitance lies below 10 μF cm^{-2} for all BT-B concentrations and this indicates that the additive is very substantially adsorbed. In the region between 0.1 and 0.6 V the decrease in capacitance resulting from BT-B addition is less dramatic and this may be related to a competitive adsorption between adsorbed anions (chloride, sulphate and/or bisulphate) and the adsorbed additive.

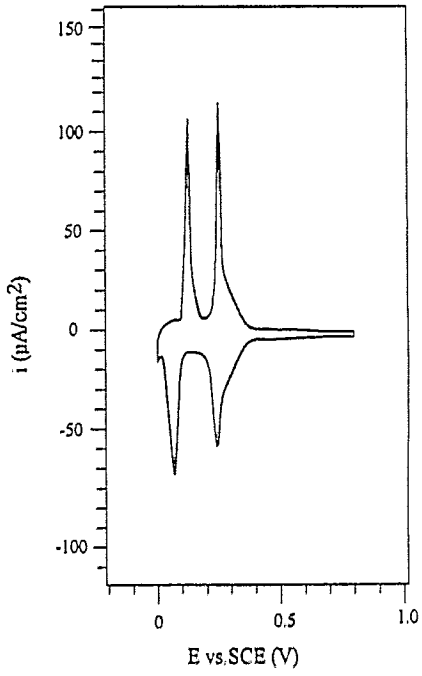

Fig. 6. A cyclic voltammogram of Au(111) in 0.1M H_2SO_4 + 1mM $CuSO_4$. Potentials vs. SCE, scan rate: 0.02 V/s.

3.1.2. Cyclic voltammetry of copper UPD on Au(111) in sulphuric acid base electrolytes with and without BT-B

Cyclic voltammetry was also used to characterise the underpotential deposition of Cu on Au(111) in the presence of BT-B. In Fig. 6 we show a cyclic voltammogram of Au(111) in 0.1 H_2SO_4 + 1mM $CuSO_4$, which is in good agreement with that previously reported in the literature [21]. Two distinctive peaks are observed, which have been well characterised and assigned to the formation of an ordered $(\sqrt{3} \times \sqrt{3})$R30° copper adlayer (honeycomb structure) for medium coverages and a (1×1) superstructure for the complete monolayer [10]. Integration of both peaks gives a charge of 430 μC cm^{-2}, which is close to that predicted for the adsorption and full discharge of a complete monolayer of Cu in a (1×1) adlayer. Indeed, this monolayer has been characterised by a variety of techniques including EXAFS [7], in-situ atomic force microscopy (AFM) [9] and in-situ X-ray spectroscopy [8]. These techniques show that the complete UPD monolayer has a (1×1) structure, with the lateral Cu–Cu distances corresponding with those of the gold substrate.

The (1×1) ad-layer is of more relevance for this study since our SPM measurements involved first recording an image at potentials slightly positive of the Nernst potential (where the Au(111) electrode is covered by the pseudomorphic copper monolayer) and then stepping the potential to the overpotential deposition region. Hence, in this situation the UPD Cu monolayer can be assumed to be the "precursor layer" on-top of which the bulk deposit is formed.

Our initial cyclic voltammetry measurements of Cu UPD in BT-B containing electrolytes indicated that the underpotential deposition of copper in these electrolytes is extremely slow, with the Cu adlayer not being completed even at scan rates as low as 5 mV s^{-1}. Fig. 7 shows a voltammogram of Au(111) in 0.1 H_2SO_4 + 1mM $CuSO_4$ + 3×10^{-4}M BT-B. In this case a starting potential of 10 mV was chosen and this potential was held for 240 s prior to sweeping the potential in the positive direction. A sharp peak is observed at 0.435 V, which does not increase in size with increasing waiting time. This peak is assigned to the stripping of the Cu adlayer. The integration of this desorption peak gives a charge of 430 μC cm^{-2}, which is identical to that obtained in the absence of BT-B. This is an indication that a complete Cu monolayer is also formed in the presence of BT-B, although we cannot be conclusive

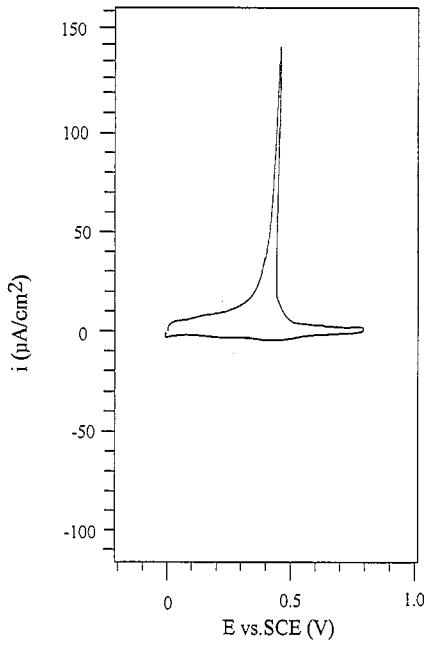

Fig. 7. A cyclic voltammogram of Au(111) in 0.1M H_2SO_4 + 1mM $CuSO_4$ with 3×10^{-4} M BT-B. Potentials vs. SCE, scan rate 0.02 V/s:

concerning this point since we do not know the electroadsorption valency of Cu for this particular electrolyte or whether additional faradaic processes occur.

Also notice that the peaks on the return sweep in Fig. 7 are very substantially depressed with respect to the forward direction. These voltammetric results show that the stripping of the copper adlayer is substantially faster than its formation. This points to a mechanism of Cu-adlayer formation, in which the organic adsorbate blocks sites for the copper deposition, which has to either "penetrate under" the adsorbed BT-B layer or (partially) displace the organic molecules. A similar mechanism has been proposed for Cu UPD on Pt(111) in the case of other organic adsorbates [22]. Since the copper stripping peaks are substantially different with and without the organic additive (compare the anodic sweeps of Figs. 6 and 7) we conclude that the organic additive is also strongly adsorbed on the Cu adlayer. This deduction is consistent with the marked effect that this additive also has on bulk copper deposition following subsequent potential steps to the OPD region (see following sections).

3.2. Scanning probe microscopy

3.2.1. Stranski–Krastanov growth (A)

As discussed in the preceding section a monolayer of copper is deposited on Au(111) at potentials slightly positive of the Nernst potential for bulk copper deposition. Upon stepping the electrode potential to potentials of bulk copper deposition three-

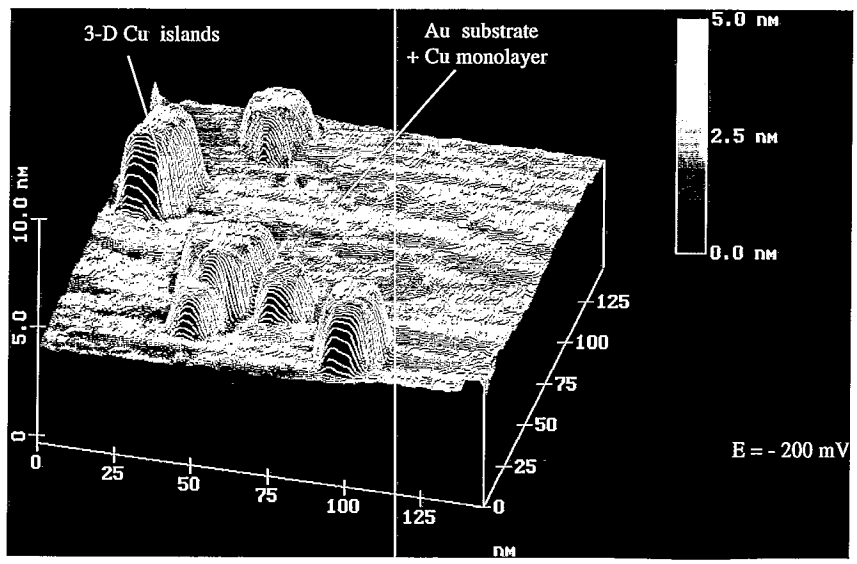

Fig. 8. An in-situ STM image of bulk copper deposition on a gold film at −200 mV (vs. Cu/Cu^{2+}) in 0.1M H_2SO_4 + 1mM $CuSO_4$.

dimensional *flat topped* copper islands are formed on-top of this monolayer. Such copper islands generally nucleate at defects in the substrate, such as step edges [23]. This can be seen in the in-situ STM image in Fig. 8, which was recorded for a gold film at −200 mV (versus Cu/Cu^{2+}) in 0.1M H_2SO_4 + 1mM $CuSO_4$. This single image has been taken from a complete series of images, in which the surface was first imaged at potentials slightly positive of the Nernst potential (where the surface is covered by the UPD Cu adlayer) and then subsequently imaged following excursions to potentials of bulk copper formation and then back again positive of the Nernst potential, where the bulk deposit is stripped. During such sequences care was taken to ensure that the same area of the surface was examined by observing characteristic features on the surface such as step edges.

The growth morphology observed in Fig. 8 is best described as Stranski–Krastanov growth. The Cu monolayer is formed at underpotentials due to the favourably strong Cu–Au bonding. This epitaxially deposited monolayer is highly strained since the Cu–Cu distance of a Cu(111) surface is significantly shorter (0.256 nm) than Au–Au for Au(111) (0.289 nm). The bulk copper deposit does not possess the energetic advantage of the strong Cu–Au bonding, as does the UPD layer. It is clear that a further perfect epitaxial deposition of bulk copper on-top of the UPD layer would lead to highly strained films. This seems the most likely reason for the quenching of the perfect epitaxial growth in favour of the formation of 3D islands and hence the observation of Stranski–Krastanov growth morphology.

3.2.2. Frank–van der Merwe Monolayer growth (B_1)

The growth of individual copper monolayers has been observed for subsequent copper deposition (in additive containing electrolytes) onto gold films which are already covered with a bulk copper film (thickness > 4–7 monolayers). Three separate monolayers growing on-top of a multilayer film can be seen in Fig. 9. In this case the growth of these monolayer islands begun before the underlying multilayer film was complete, with the monolayers growing in from the edges of the underlying multilayer film. In other cases the growth of these monolayer islands was only seen after the surface was completely covered with the multi-layer copper film [24].

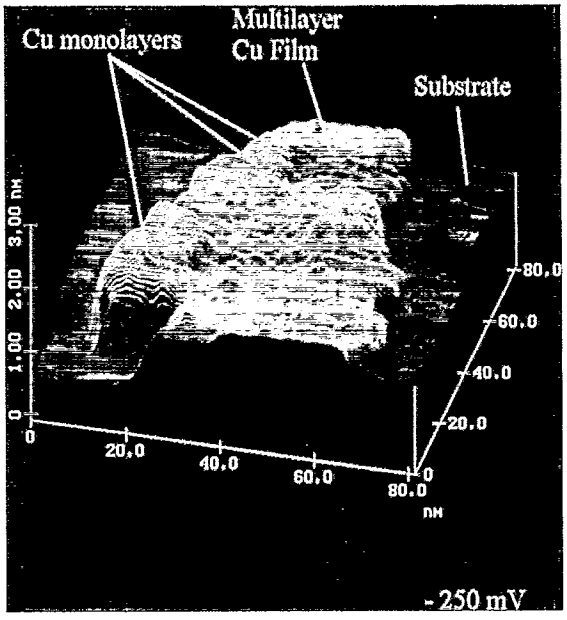

Fig. 9. An in-situ STM images of 2D monolayer Cu-deposition onto a multi-layer (quasi-2D) copper films (on a gold substrates). Electrolyte: 0.1M H_2SO_4 + 1mM $CuSO_4$ + 10 mg/l BT-B.

By contrast, formation of Cu-monolayers directly on-top of the UPD layer is not observed (a "multi"-layer film is consistently deposited – see next section). This difference between the first bulk layer and subsequent layers indicates that the "surface template" for deposition is quite different in both cases. The first bulk layer is deposited on-top of an internally strained Cu monolayer, in that the Cu–Cu distances are significantly different from those of a Cu(111) surface. An explanation would be that this strain is largely relieved by the stage that the film has reached a certain thickness (4–7 monolayers). This explanation is consistent with X-ray diffraction studies of bulk Pb deposition on Ag(111), where the Pb film restructures to alleviate strain after the deposition of approximately five monolayers of lead [26]. In the case of metal-on-metal growth from the gas phase strain phenomena are well recognised. One from many examples is Pd/Ag (100) [see Ref. [27] and references therein]. In this case Pd initially grows in perfect epitaxy, with a 5.1% lateral expansion imposed by the substrate. However, relaxation to the bulk structure occurs after about 3 monolayers.

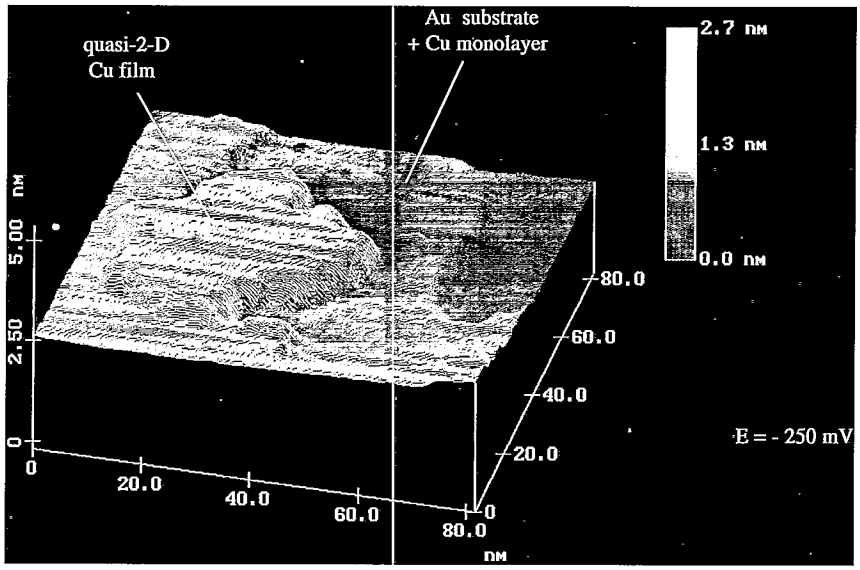

Fig. 10. In-situ STM image of Cu-deposition on a gold film from 0.1M H_2SO_4 1mM $CuSO_4$ + 10 mg/1 BT-B.

3.2.3. Frank–van der Merwe Multilayer film growth (B_2)

The growth of ultra-thin, but not monolayer, films is observed for the deposition of the first bulk copper layer on-top of UPD covered Au(111) surfaces in the presence of additives such as BT-B [24,25]. The copper clusters, which are formed directly following a potential step to negative potentials, grow at almost

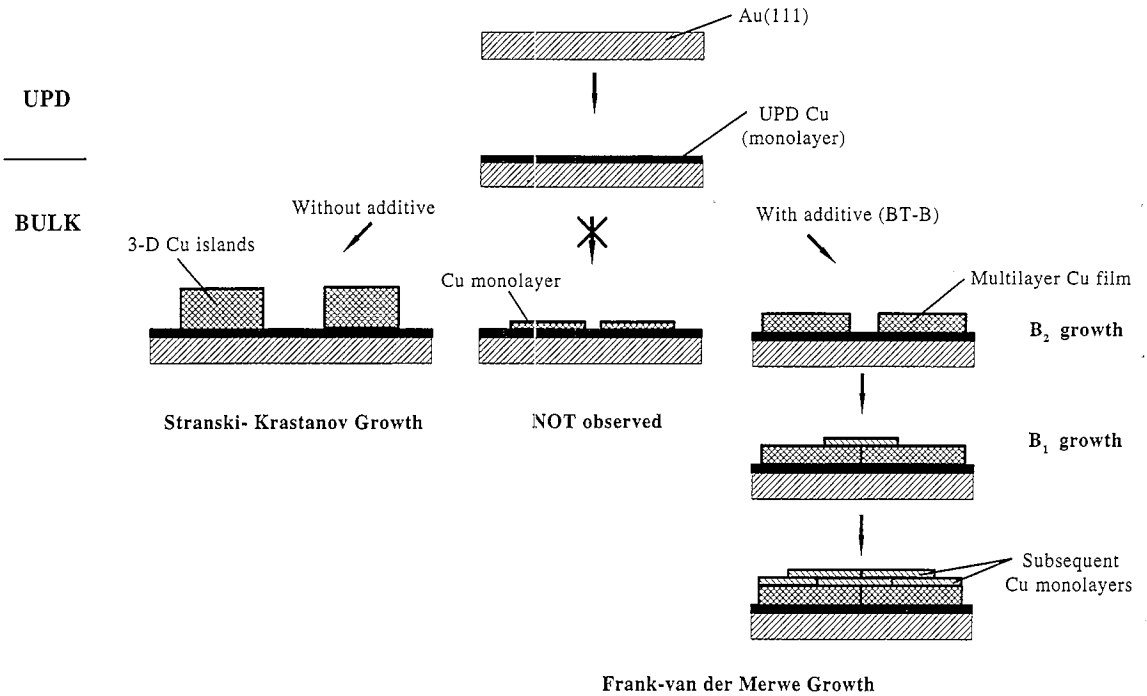

Fig. 11. A schematic representation of the electrodeposition of copper on Au(111) with and without BT-B addition.

Table 1
Summary of observations for bulk copper deposition onto gold and polypyrrole electrodes: Base electrolyte: 0.1M H_2SO_4 + 1mM $CuSO_4$

Substrate	Additive	Growth morphology	Growth mechanism
UPD Cu/Au(111)	None	3D	Stranski–Krastanov
UPD Cu/Au(111)	BT-B	quasi 2D	Frank–Van der Merwe (B_2)
Subsequent Cu deposition on Au substrates precovered with a Cu multilayer film	BT-B	2D	Frank–Van der Merwe (B_1)
Polypyrrole	None	3D	Volmer–Weber
Polypyrrole	BT-B	3D	Volmer–Weber

constant height laterally across the surface (quasi-2D growth), typically reaching a height of up to 4–7 monolayers. The organic additive severely inhibits the vertically propagation of the individual copper crystallites in favour of their lateral spreading. Such a multi-layer film can be seen in Fig. 10.

These observations are pictorially summarised in Fig. 11, for the deposition of bulk copper on-top of UPD covered Au(111) substrates in the presence and absence of the additives.

3.2.4. *Volmer–Weber growth (C)*

Volmer–Weber growth has been observed for copper deposition on conductive polypyrrole (PPy) electrodes, both in the presence and absence of additives. In Fig. 12a, 3D copper clusters can be readily distinguished on-top of the polypyrrole substrate. A comparable morphology for the copper growth is also observed in the presence of BT-B (Fig. 12b).

Volmer–Weber growth is generally observed for adsorption on surfaces, where the adsorbate–substrate interaction is relatively weak. Such a situation favours the formation of 3D islands. Even an additive such as BT-B, which promotes a quasi-2D growth of Cu on Au, is not able to overcome the presumably weaker Cu–PPy interaction and is unable to promote 2D growth of Cu on polypyrrole.

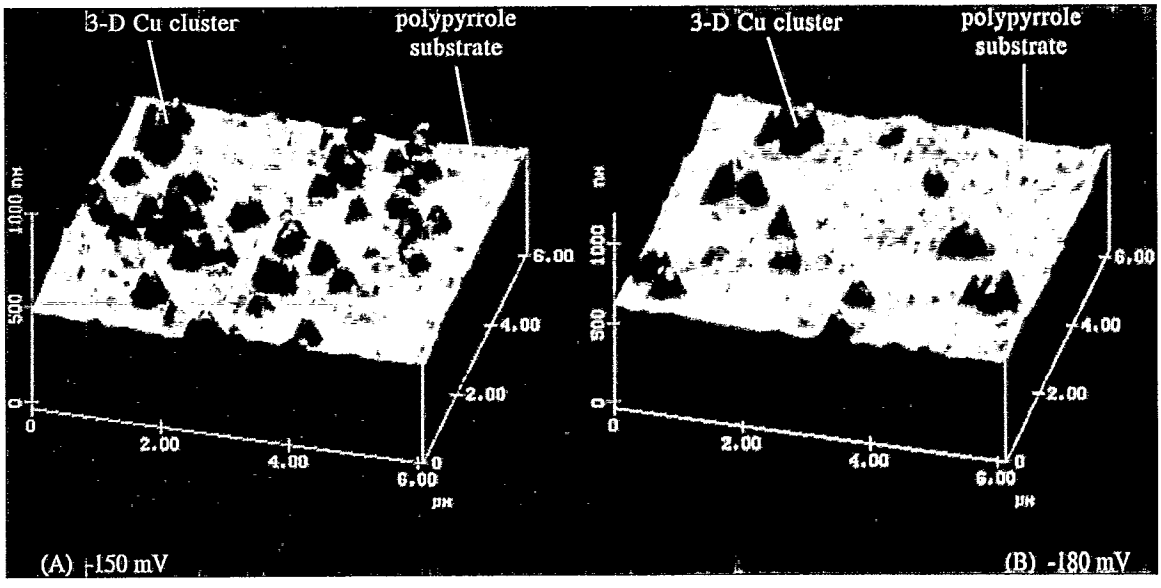

Fig. 12. In-situ AFM images of Cu-deposition on a conductive polypyrrole from 0.1M H_2SO_4 + 1mM $CuSO_4$ (a) without additive and (b) with 10 mg/l BT-B.

4. Summary

We have classified the growth modes for *bulk* copper on-top of:

- Au(111) "precovered" with UPD-Cu;
- multilayer copper films (on Au(111));
- polypyrrole;

in the absence and presence of organic additives. The results are summarised in Table 1. The models used to rationalise the observed growth behaviours are based on thermodynamic arguments, which predict growth morphology in terms of deposit–substrate interaction and strain arising from misfit. The simple thermodynamic models fit the observations well.

References

[1] E. Bauer, Z. Kristallogr. 110 (1958) 372.
[2] NATO ASI, Proceedings of Nanoscale Probes of the Solid/Liquid Interface, Eds. H. Siegenthaler and A. Gewirth (Kluwer, Dordrecht, 1995).
[3] E.B. Budevski, in: Comprehensive Treatise of Electrochemistry, Vol. 7, Eds. B.E. Conway, J.O. Bockris, E. Yeager, S.U.M. Khan and R.E. White (Plenum, New York, 1984) pp. 399–450.
[4] I. Markov and S. Stoyanov, Contemp. Phys. 28 (1987) 267.
[5] W. Obretenov, U. Schmidt, W.J. Lorenz, G. Staikov, E. Budevski, D. Carnal, U. Müller, H. Siegenthaler and E. Schmidt, J. Electrochem. Soc. 140 (1993) 692.
[6] G. Staikov, E. Budevski, W. Obretenov and W.J. Lorenz, J. Electroanal. Chem. 349 (1993) 335.
[7] O.R. Melroy, M.G. Samant, G.L. Borges, J.G. Gordon, L. Blum, J.H. White, M.J. Albarelli, M. McMillan and H.D. Abruna, Langmuir 4 (1988) 728.
[8] A. Tadjeddine, D. Guay, M. Ladouceur and G. Tourillon, Phys. Rev. Lett. 66 (1991) 2235.
[9] N. Ikemiya, S. Miyaoka and S. Hara, Surf. Sci. 311 (1994) L641.
[10] Y. Nakai, M.S. Zei, D.M. Kolb and G. Lehmpfuhl, Ber. Bunsenges. Phys. Chem. 88 (1984) 340.
[11] J. Clavilier, R. Faure, G. Guinet and R. Durand, J. Electroanal. Chem. 107 (1980) 205.
[12] D.M. Kolb, R.J. Nichols and R.J. Behm, in: Electrified Interfaces in Physics, Chemistry and Biology, Ed. R. Guidelli, NATO ASI Series C (Kluwer, Dordrecht, 1992) p. 275.
[13] T.R.I. Cataldi, I.G. Blackham, G.A.D. Briggs, J.B. Pethica and H.A.O. Hill, J. Electroanal. Chem. 290 (1990) 1.
[14] W. Haiss, D. Lackey, J.K. Sass and K.H. Besocke, J. Chem. Phys. 95 (1991) 2193.
[15] H. Angerstein-Koslowska, and B.E. Conway, A. Hamelin and L. Stoicoviciu, J. Electroanal. Chem. 228 (1987) 429.
[16] D.M. Kolb and J. Schneider, Electrochim. Acta 31 (1986) 929.
[17] A. Friedrich, B. Pettinger, D.M. Kolb, G. Lübke, R. Steinhoff and G. Marowsky, Chem. Phys. Lett. 163 (1989) 123.
[18] J. Wang, B.M. Ocko, A.J. Davenport and H.S. Isaacs, Phys. Rev. B 46 (1992) 10321.
[19] X. Gao, A. Hamelin and M.J. Weaver, J. Chem. Phys. 95 (1991) 6993.
[20] N.J. Tao and S.M. Lindsay, Surf. Sci. 274 (1992) L546.
[21] D.M. Kolb, K. Al Jaaf-Golze and M.S. Zei, DECHEMA-Monographien, Vol. 12 (Verlag Chemie, Weinheim, 1986) p. 53.
[22] A.S. Dakkouri, N. Batina and D.M. Kolb, Electrochimica Acta 38 (1993) 2467.
[23] R.J. Nichols, D.M. Kolb and R.J. Behm, J. Electroanal. Chem. 313 (1991) 109.
[24] R.J. Nichols, C.E. Bach and H. Meyer, Ber. Bunsenges, Phys. Chem. 97 (1993) No. 8, 1012.
[25] R.J. Nichols, W. Beckmann, H. Meyer, N. Batina and D.M. Kolb, J. Electroanal. Chem. 330 (1992) 381.
[26] O.R. Melroy, M.F. Toney, G.L. Borges, M.G. Samant, J.B. Kortright, P.N. Ross and L. Blum, J. Electranal. Chem. 285 (1989) 403.
[27] G.A. Somorjai, Introduction to Surface Chemistry and Catalysis (Wiley, New York, 1994) p. 60.